SVPWM Strategy of Matrix Converter Fed Asymmetrical Six-phase Induction Motor With Common-mode Voltage Elimination and Unity Power-factor Operation

Sayan Paul
Dept. of Electrical Engineering
Indian Institute of Science
Bangalore, India
sayanp@iisc.ac.in

Kaushik Basu
Dept. of Electrical Engineering
Indian Institute of Science
Bangalore, India
kbasu@iisc.ac.in

***Abstract*—Asymmetrical six-phase induction machine (ASIM) with six balanced phases and two isolated neutral points require modulation in two orthogonal two-dimensional subspaces where one of them is associated with electromechanical energy transfer. Excitation of non-energy transferring subspace causes copper loss. Therefore, this paper proposes a novel space-vector based PWM strategy (SVPWM) of matrix converter (MC) fed ASIM where excitation in non-energy transferring plane is kept as zero and energy transferring plane is excited so as to generate ripple-free torque. Eighteen switching states of $3\phi-6\phi$ MC are used for this purpose which have zero common-mode voltage. Theoretical analysis shows that the input power-factor for this technique is same as the load power-factor. Finally, a new PWM strategy is proposed to operate the MC at unity power-factor at input. The proposed techniques are verified through simulations in Matlab and experiments on 3 kW hardware prototype.**

***Index Terms*—Asymmetrical six-phase machine, Matrix Converter, space-vector modulation, common-mode voltage elimination**

I. Introduction

Asymmetrical six-phase induction machine (ASIM), one of the most popular multi-phase machines, is attractive in high power applications due to its phase-redundancy and consequently higher fault tolerance, reduced ratings of per-phase power-electronic drive unit, less susceptibility towards excitation harmonics, [1]. ASIM has two sets of balanced three-phase (3ϕ) windings in stator, which are spatially shifted by 30° (electrical), as shown in Fig. 1. Matrix converter (MC) synthesizes output voltages of controllable amplitude and frequency from the input 3ϕ voltages without bulky and unreliable storage capacitor in between and hence improves the power-density and reliability, [2]. Input unity power-factor (UPF) operation of MC is one of the desired objectives to improve the efficiency of the overall drive system. The high frequency common-mode voltage has detrimental effect on motor bearing and causes conducted EMI in electric-drive system, [3], [4]. This paper proposes a space-vector based PWM (SVPWM) strategy of MC fed ASIM with zero common-mode voltage and has the capability of UPF operation at input.

The transformation matrix, T, which is used for the modeling of ASIM, analyses the machine in three two-dimensional orthogonal subspaces, namely, $\alpha-\beta$, z_1-z_2 and o_1-o_2, [5]. With this transformation, it can be shown that $\alpha-\beta$ plane is associated with electromechanical energy transfer whereas excitation of z_1-z_2 and o_1-o_2 planes causes unwanted copper loss without contributing towards torque production. Linear modulation techniques of voltage source inverter fed ASIM are discussed in the literature where excitations in non-energy transferring planes, z_1-z_2 and o_1-o_2, are kept zero, [5]–[8]. Existing inverter fed overmodulation techniques of ASIM inject harmonic voltages in z_1-z_2 plane in order to attain higher voltage gain in $\alpha-\beta$ plane, [9]–[11]. Voltage injection in o_1-o_2 plane is not possible for ASIM with two isolated neutral points, as shown in Fig. 1. Although modulations of MC fed 3ϕ open end machine, [12], five-phase machine, [13], are explored before, modulation of MC fed ASIM still remains mostly unexplored.

Each $3\phi-3\phi$ MC has 27 permissible switching states, [2]. As $3\phi-6\phi$ MC of Fig. 1 has two $3\phi-3\phi$ MC units, 27×27 permissible switching states are there. In this paper, modeling of $3\phi-6\phi$ MC is discussed with respect to transformation T for 18 switching states which produce zero common-mode voltages between supply neutral and machine neutral points ($v_{on}=v_{o'n}=0$). These states generate synchronously rotating voltage space-vectors of fixed length in both $\alpha-\beta$ and z_1-z_2 subspaces and zero voltage vectors in o_1-o_2 plane. Based on the direction of rotation of the resultant space-vectors in $\alpha-\beta$ plane, the switching states are divided into two groups. Two novel SVPWM strategies, one for each of these groups, are presented in this paper which have the following features.

- Balanced sinusoidal voltage excitation in $\alpha-\beta$ plane to generate ripple-free torque.
- Zero average voltage injection in z_1-z_2 and o_1-o_2 planes to achieve higher drive efficiency. Therefore, the proposed strategies are linear modulation techniques of

978-1-7281-5826-6/20/$31.00 ©2020 IEEE

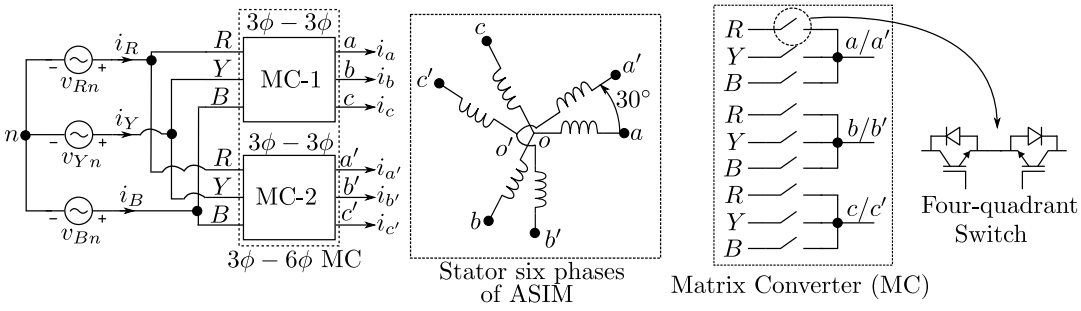

Fig. 1: $3\phi-6\phi$ matrix converter fed asymmetrical six-phase induction machine

MC fed ASIM.

- Instantaneous zero common-mode voltage between supply neutral and machine neutrals.

It is shown through theoretical analysis that the input power-factors for both of these techniques are same as load power-factor. Finally, a new PWM strategy is proposed that uses both of the two groups to maintain the input power-factor at unity.

The organization of the paper is as follows. Section II briefly discusses the modeling of both machine and converter with respect to transformation matrix T. With respect to these models, linear modulation techniques and input current analysis of MC fed ASIM are discussed in section III. The proposed techniques are validated through experiments and simulations in section IV and the paper is concluded in section V.

II. Modeling of ASIM and MC

Fig. 1 shows $3\phi-6\phi$ matrix converter (MC) fed asymmetrical six-phase induction machine (ASIM). Six stator windings of ASIM are connected in star fashion with two isolated neutral points, o and o'. Six terminals of ASIM, a, b,..c', are directly connected to six poles of 6ϕ MC. The 6ϕ MC consists of two $3\phi-3\phi$ MCs, MC-1 and MC-2, respectively. Each of these MCs has nine four-quadrant switches arranged in matrix form, as shown in Fig. 1. Suppose, the input balanced 3ϕ voltages are given by (1).

$$v_{Rn}=V_i\cos\omega_i t;\qquad v_{Yn}=V_i\cos\left(\omega_i t-\frac{2\pi}{3}\right);$$
$$v_{Bn}=V_i\cos\left(\omega_i t-\frac{4\pi}{3}\right) \tag{1}$$

Equation (2) shows a standard 6×6 transformation matrix, T, which is used for modeling of ASIM, [5]. Here, Tr denotes transpose operation. T transforms quantities from original domain to three two-dimensional orthogonal subspaces, namely, $\alpha-\beta$, z_1-z_2, and o_1-o_2. With balanced six-phase windings of ASIM and two isolated neutrals, o_1-o_2 plane can't be excited and hence, it is excluded from further discussion. $\alpha-\beta$ plane is associated with electromagnetic energy transfer and equivalent circuit in this plane is similar to the equivalent circuit of 3ϕ induction machine (IM). The equivalent circuit in z_1-z_2 plane consists of series connected winding resistance and leakage inductance. Therefore, impedance in the z_1-z_2 plane is small. Small voltage excitation in this plane results into large current which causes unnecessary copper loss without generating torque. Therefore, average synthesized voltages in this plane should be zero. Dynamic equivalent circuits in $\alpha-\beta$ and z_1-z_2 planes are decoupled in nature.

TABLE I: Switching States of $3\phi-3\phi$ MC With Zero Common-mode Voltage

State	Label	State	Label	State	Label
RYB	1	YBR	3	BRY	5
RBY	2	YRB	4	BYR	6

$$X_i \triangleq \underbrace{\frac{1}{\sqrt{3}}\begin{bmatrix} 1 & -\frac{1}{2} & -\frac{1}{2} & \frac{\sqrt{3}}{2} & -\frac{\sqrt{3}}{2} & 0\\ 0 & \frac{\sqrt{3}}{2} & -\frac{\sqrt{3}}{2} & \frac{1}{2} & \frac{1}{2} & -1\\ 1 & -\frac{1}{2} & -\frac{1}{2} & -\frac{\sqrt{3}}{2} & \frac{\sqrt{3}}{2} & 0\\ 0 & -\frac{\sqrt{3}}{2} & \frac{\sqrt{3}}{2} & \frac{1}{2} & \frac{1}{2} & -1\\ 1 & 1 & 1 & 0 & 0 & 0\\ 0 & 0 & 0 & 1 & 1 & 1 \end{bmatrix}}_{T} X_j$$
$$X_i=\begin{bmatrix} x_\alpha & x_\beta & x_{z_1} & x_{z_2} & x_{o_1} & x_{o_2}\end{bmatrix}^{Tr}$$
$$X_j=\begin{bmatrix} x_a & x_b & x_c & x_{a'} & x_{b'} & x_{c'}\end{bmatrix}^{Tr} \tag{2}$$

Each $3\phi-3\phi$ MC has six possible switching states with common-mode voltages, v_{on} or $v_{o'n}$, zero, [12]. These states are labelled by the input three phases, R, Y, and B, in the order they are connected to the three output ports, a/a', b/b', and c/c', respectively. These states are re-labelled in Table I for brevity. As each of MC-1 and MC-2 has 6 switching states with zero common-mode voltage, $3\phi-6\phi$ MC of Fig. 1 has $6\times6=36$ possible states. These states are labelled by an ordered pair of the form (x,y'), where x and y are the states of MC-1 and MC-2, respectively and $x,y\in\{1,2..6\}$. Therefore, state $(5,3')$ of 6ϕ MC implies switching state of MC-1 is 5 and that of MC-2 is 3. According to Table I, it means pole a is connected to input phase B, i.e., $a-B$, $b-R$, $c-Y$, $a'-Y$, $b'-B$ and $c'-R$.

To model this 6ϕ MC with T, the line-neutral voltages of

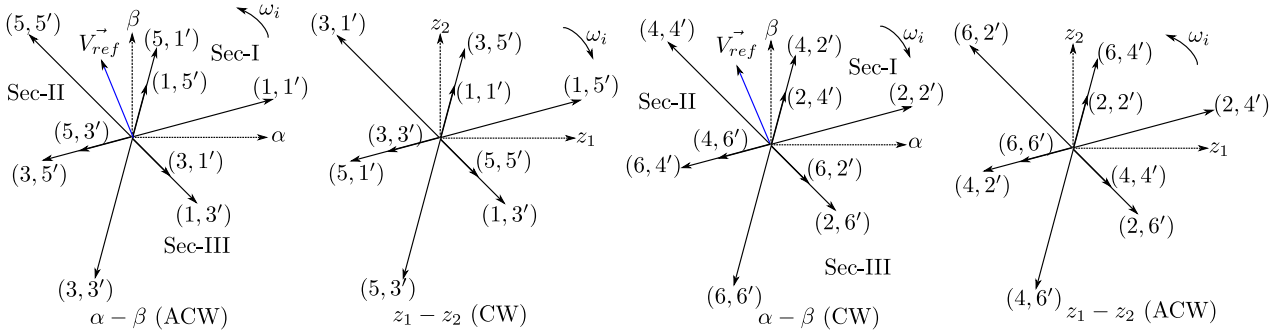

(a) 9 states with odd combinations (b) 9 states with even combinations

Fig. 2: Mapping of 18 switching states of 6ϕ MC

ASIM, i.e., v_{ko} and $v_{k'o'}$ where $k \in \{a, b.c\}$, generated by the switching states of the converter need to be determined first. Thereafter, T is applied on these line-neutral voltages to get the voltages generated by the switching states in $\alpha - \beta$ and $z_1 - z_2$ subspaces. Applying KVL on the loop formed by machine terminal to machine neutral to supply neutral, (3) is obtained. For aforementioned 36 states, $v_{on} = v_{o'n} = 0$ and therefore, $v_{ko} = v_{kn}$ and $v_{k'o'} = v_{k'n}$, $k \in \{a, b.c\}$. For example, $(5, 3')$ gives $v_{ao} = v_{an} = v_{Bn}$, as pole a is connected to input phase B, $v_{bo} = v_{Rn}$, $v_{co} = v_{Yn}$, $v_{a'o'} = v_{Yn}$, $v_{b'o'} = v_{Bn}$, $v_{c'o'} = v_{Rn}$.

$$v_{ko} = v_{kn} + v_{no}; \quad v_{k'o'} = v_{k'n} + v_{no'}; \quad k \in \{a, b.c\} \tag{3}$$

When T is applied on the line-neutral voltages generated by the states of the form (x, y'), with both x and y odd, synchronously rotating space-vectors of constant amplitudes are generated in both $\alpha - \beta$ and $z_1 - z_2$ subspaces. Application of T on the line-neutral voltages generated by our example switching state, $(5, 3')$, result into $v_\alpha + jv_\beta = \sqrt{3}V_i \cos 75° e^{j(\omega_i t - 165°)}$; $v_{z_1} + jv_{z_2} = \sqrt{3}V_i \cos 15° e^{-j(\omega_i t + 105°)}$, after substituting $v_{Rn,Yn,Bn}$ from (1). These space-vectors rotate anti-clockwise (ACW) in $\alpha - \beta$ and CW in $z_1 - z_2$ plane. Similar conclusion can be made for both x and y even; here directions of rotation in both of these subspaces are opposite. The combinations of even and odd states of MC-1 and MC-2, e.g. $(5, 4')$ or $(4, 5')$, give rise to stationary space-vectors of time-varying amplitudes in both the subspaces. These vectors are not considered in this paper for modulation of MC-fed ASIM. Therefore, 18 switching states, 9 states with odd and 9 states with even combinations, are used for modulation of ASIM out of 36 possible states. Fig. 2 shows the mapping of these 18 states in $\alpha - \beta$ and $z_1 - z_2$ subspaces. Space-vectors generated by these states are of three different lengths. The lengths of the large, medium and small vectors, denoted by L, M and S, respectively, are given in (4). The states with largest vectors in $\alpha - \beta$ plane have smallest lengths in $z_1 - z_2$ and vice-versa. States with length M in $\alpha - \beta$ have length M in $z_1 - z_2$ plane as well.

$$L = \sqrt{3}V_i \cos 15°, M = \sqrt{3}V_i \cos 45°, S = \sqrt{3}V_i \cos 75° \tag{4}$$

III. Modulation of MC Fed ASIM

As $\alpha - \beta$ plane is responsible for energy transfer, it should be excited with balanced fundamental voltage like 3ϕ IM, as given in (5a). Here, bar represents the average value over a switching cycle. The factor $\sqrt{3}$ is introduced so that inverse transformation of (2) results into amplitudes of line-neutral voltages equal to V_o. Let, the modulation index, m_I, be defined as $m_I \triangleq \frac{V_o}{V_i}$. As excitation of $z_1 - z_2$ planes causes unwanted copper loss, reference voltages in $z_1 - z_2$ plane are zero, as given in (5b).

$$\vec{V_{ref}} \triangleq \overline{v}_\alpha + j\overline{v}_\beta = \sqrt{3}V_o e^{j\omega_o t} = \sqrt{3}m_I V_i e^{j\omega_o t} \tag{5a}$$

$$\overline{v}_{z_1} + j\overline{v}_{z_2} = 0 \tag{5b}$$

In order to satisfy these four voltage constraints in $\alpha - \beta - z_1 - z_2$ planes along with the duty ratio constraint, i.e., summation of all duty ratios is 1; at least five vectors need to be applied. This paper proposes the application of 2 large and 3 medium vectors (2L+3M), nearest to the reference voltage vector in $\alpha - \beta$, $\vec{V_{ref}}$, due to the following reasons:

1) 2 Large vectors, adjacent to $\vec{V_{ref}}$, will help to achieve higher m_I.
2) 3 large vectors are not applied as the error voltage vector due to the farthest large vector from $\vec{V_{ref}}$ will cause higher current ripple in $\alpha - \beta$ plane.
3) Small vectors are not applied in $\alpha - \beta$ plane as they result into large voltage vectors in $z_1 - z_2$ plane. As the reference voltage vector in this subspace is zero, the error voltage vector is equal to these large voltage vectors which cause higher current ripple in $z_1 - z_2$ plane.

Three large vectors in $\alpha - \beta$ plane divides the plane in three sectors, as shown in Fig. 2. Based on the location of tip of $\vec{V_{ref}}$

in one of these three sectors, 2 adjacent large vectors along with 3 medium vectors are used. $\vec{V_{ref}}$ can be synthesized either by using ACW rotating states or using CW rotating states of $\alpha-\beta$.

A. Modulation with ACW rotating states of $\alpha-\beta$

Suppose, $\vec{V_{ref}}$ is in sector-I in $\alpha-\beta$ plane, as shown in Fig. 2a. Following the aforementioned strategy, two adjacent large vectors, $(1,1')$, $(5,5')$, and all medium vectors of $\alpha-\beta$ are chosen. If D_1, D_2,...D_5 are the duty ratios for which states $(1,3')$, $(1,1')$, $(5,1')$, $(5,5')$ and $(3,5')$ are applied, respectively, in order to synthesize $\vec{V_{ref}}$ in $\alpha-\beta$ and zero vector in z_1-z_2, the expressions of D_1-D_5 can be determined after solving the set of equations given in (6). The left-hand sides of (6a) and (6b) are the algebraic summation of the product of dwell times and the space-vectors generated by the switching states in $\alpha-\beta$ and z_1-z_2 planes, respectively and therefore, they represent the average voltages generated by the set of 5 aforementioned switching states in $\alpha-\beta$ and z_1-z_2 planes, respectively. These synthesized average voltages are equated with desired voltages of these planes, as given in (5), to obtain the duty ratios. For example, the space-vectors generated by $(1,1')$ in $\alpha-\beta$ and z_1-z_2 are $Le^{j(\omega_i t+15^\circ)}$ and $Se^{-j(\omega_i t-75^\circ)}$. As $(1,1')$ is applied for D_2 duty ratio, these vectors multiplied with D_2 appear as the second terms in left-hand sides of (6a) and (6b). Equation (6c) equates the summation of all the duty ratios to 1.

$$e^{j\omega_i t}(D_1 M e^{-j45^\circ}+D_2 L e^{j15^\circ}+D_3 M e^{j75^\circ} + D_4 L e^{j135^\circ}+D_5 M e^{j195^\circ})=\vec{V_{ref}}=\sqrt{3}m_I V_i e^{j\omega_o t}; \tag{6a}$$

$$e^{-j\omega_i t}(D_1 M e^{-j45^\circ}+D_2 S e^{j75^\circ}+D_3 M e^{j195^\circ} + D_4 S e^{-j45^\circ}+D_5 M e^{j75^\circ})=0; \tag{6b}$$

$$\sum_{i=1}^{5} D_i = 1 \tag{6c}$$

The expressions of D_1-D_5 in terms of m_I and $\theta=(\omega_o-\omega_i)t$ are given in (7). To make these duty ratios feasible for practical implementation, $D_i \geq 0, \forall i=1,2..5$ in the range of $15^\circ \leq \theta \leq 135^\circ$, i.e., in sector-I. In order to satisfy these five inequality constraints in sector-I, m_I should lie in the range $0 \leq m_I \leq 0.5$. Therefore, the maximum modulation index achievable with this strategy is 0.5. Modulation in other two sectors can be performed in the similar manner.

$$D_1=\frac{1}{3}-\frac{2}{3}m_I\sin(\theta); \quad D_2=\frac{2\sqrt{2}}{3}m_I\sin(\theta+45^\circ);$$
$$D_3=\frac{1}{3}-\frac{2\sqrt{2-\sqrt{3}}}{3}m_I\sin(\theta+15^\circ);$$
$$D_4=\frac{2\sqrt{2}}{3}m_I\sin(\theta-15^\circ); \quad D_5=\frac{1}{3}-\frac{2}{3}m_I\sin(\theta+30^\circ); \tag{7}$$

B. Modulation with CW rotating states of $\alpha-\beta$

For the given $\vec{V_{ref}}$ in sector-I of $\alpha-\beta$ plane, states $(2,6')$, $(2,2')$, $(4,2')$, $(4,4')$ and $(6,4')$ can be applied in the similar way, as above, to synthesize the reference voltage vectors. Duty ratios of these states can be determined in similar fashion and maximum m_I attainable by this strategy is also 0.5. In this case, duty ratios can be expressed as functions of m_I and $(\omega_o+\omega_i)t$.

C. Input current analysis and unity power-factor operation

As the equivalent circuit of ASIM in $\alpha-\beta$ plane is similar to equivalent circuit of 3ϕ IM; excitation of $\alpha-\beta$ plane with average voltage vector of $\sqrt{3}V_o e^{j\omega_o t}$, as given in (5a), will cause average current vector, $\bar{i}_\alpha+j\bar{i}_\beta=\sqrt{3}I_o e^{j(\omega_o t+\phi_o)}$, to flow in this plane in steady-state; ϕ_o is power-factor angle of ASIM. As $\overline{v}_{z_1}+j\overline{v}_{z_2}=0$; $\bar{i}_{z_1}+j\bar{i}_{z_2}=0$. Applying inverse transformation of (2) on these average currents in transformed domains; one can get the average line currents, $\bar{i}_a$, $\bar{i}_b$,..$\bar{i}_{c'}$. Expressions of $\bar{i}_a$, $\bar{i}_{a'}$ are given in (8); $\bar{i}_b$, $\bar{i}_{b'}$ and $\bar{i}_c$, $\bar{i}_{c'}$ are phase-shifted by 120° and 240° w.r.t. $\bar{i}_a$, $\bar{i}_{a'}$. With the example case of section-III-A where $\vec{V_{ref}}$ is in sector-I; input R phase is connected to output a phase for D_1+D_2 duty ratio when $(1,3')$ and $(1,1')$ are applied. Similarly, it can be seen that input R phase is connected to output b, c, a', b' c' phases for D_3+D_4, D_5, D_2+D_3, D_4+D_5 and D_1 duty ratios, respectively. Therefore, the average input current impressed upon R phase by ACW rotating states, $\bar{i}_{R,ACW}$, can be determined as (9). Here, duty ratios D_1 to D_5 are replaced by the expressions given in (7). Input R phase current with CW rotating states can be found in the similar way and is given in (10). Y and B phase currents are phase shifted by 120° and 240° with respect to R-phase current. These expressions of input currents are independent of the sector. It can be seen that the average input current is of same frequency with input voltage. But the input power-factor angles generated by ACW and CW rotating states are same and opposite, respectively, to ϕ_o. By applying both ACW and CW rotating states within a sampling period, T_s, and dividing T_s equally between them; unity power-factor operation is achieved, as shown in (11), where $\bar{i}_{R,UPF}$ is in same phase with v_{Rn}. The amplitude of the input current, $\bar{i}_{R,UPF}$, is modified with the load power-factor.

$$\bar{i}_a=I_o\cos(\omega_o t+\phi_o); \quad \bar{i}_{a'}=I_o\cos\left(\omega_o t+\phi_o-\frac{\pi}{6}\right) \tag{8}$$

$$\begin{aligned}\bar{i}_{R,ACW}=&(D_1+D_2)\bar{i}_a+(D_3+D_4)\bar{i}_b+D_5\bar{i}_c \\ &+(D_2+D_3)\bar{i}_{a'}+(D_4+D_5)\bar{i}_{b'}+D_1\bar{i}_{c'} \\ &=2m_I I_o\cos(\omega_i t+\phi_o)\end{aligned} \tag{9}$$

$$\bar{i}_{R,CW}=2m_I I_o\cos(\omega_i t-\phi_o); \tag{10}$$

$$\bar{i}_{R,UPF}=\frac{1}{2}(\bar{i}_{R,ACW}+\bar{i}_{R,CW})=2m_I I_o\cos\phi_o\cos\omega_i t; \tag{11}$$

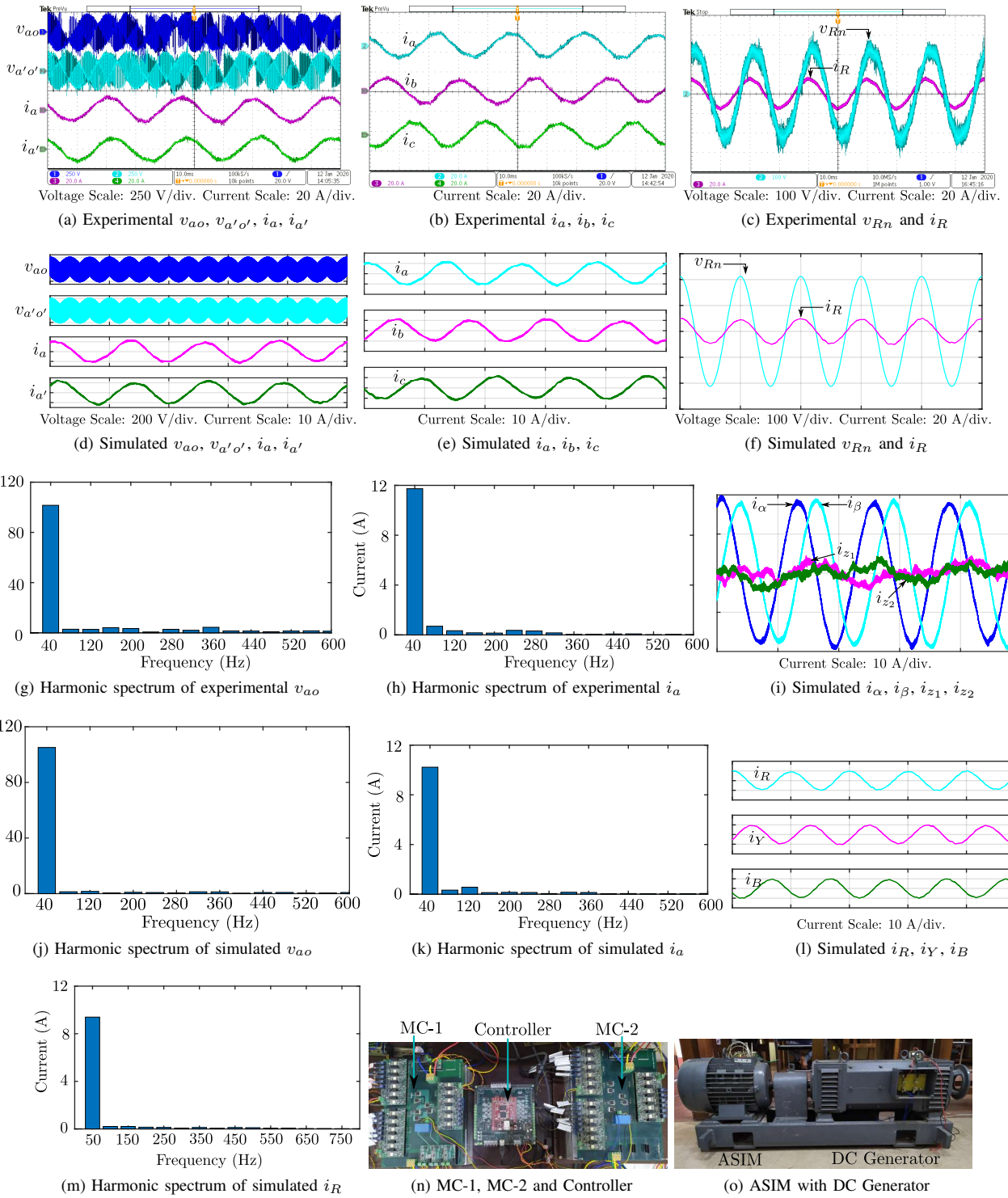

Fig. 3: Hardware set-up and experimental and simulated waveforms of proposed technique at $m_I = 0.5$; Time Scale of experimental waveforms=10 ms/div., Time Scale of simulated waveforms=20 ms/div.

TABLE II: Steady-state Equivalent Circuit Parameters of 6ϕ IM

Per phase stator and rotor resistances	0.675 Ω
Per phase stator and rotor leakage inductances	3.75 mH
Per phase magnetizing inductance	0.168 H

TABLE III: Operating Conditions of Experiments and Simulations

Peak input line-neutral voltage (V_i)	$150\sqrt{2}$ V
Input frequency (ω_i)	100π rad/sec
Output frequency (ω_o)	80π rad/sec
Modulation index (m_I)	0.5
Input power	3 kW
Sampling Frequency ($\frac{1}{T_s}$)	5 kHz

IV. Simulation and Experimental Results

The proposed technique is validated through experiment and simulation on 3 kW hardware prototype. Fig. 3o shows 2 pole ASIM which is coupled with DC generator for loading purpose. The steady-state equivalent circuit parameters of ASIM are given in Table II. Fig. 3n shows discrete IGBT (IKW40N120H3) based MC-1 and MC-2 and Zynq-7010 based controller card which have been used during experiment. Dynamic model of ASIM is implemented in Matlab Simulink to verify the proposed technique. Fig. 3 shows both experimental and simulated results for the operating condition given in Table III.

Fig. 3a and 3d show experimental and simulated output line-neutral voltages v_{ao}, $v_{a'o'}$; and line currents i_a and $i_{a'}$. Both voltage and current waveforms of a' phase are shifted by 30° w.r.t. voltage and current waveforms of a phase. Two sets of 3ϕ line currents of ASIM, i_a, i_b, i_c and $i_{a'}$, $i_{b'}$, $i_{c'}$, are balanced sinusoids which are phase-shifted by 120° w.r.t. each other. Experimental and simulated waveforms of one such set of 3ϕ current are shown in Fig. 3b and 3e, respectively. Waveform of other set looks similar to it and hence, is not shown here. Fig. 3i shows the resultant $\alpha-\beta$ and z_1-z_2 plane current waveforms corresponding to simulation. The sinusoidal $\alpha-\beta$ plane currents ensure the ripple-free torque operation of ASIM. Although z_1-z_2 plane currents are not zero, as it should be in ideal case, their magnitudes are small compared to currents in $\alpha-\beta$ plane. Fig. 3g and 3j show the harmonic spectra of experimental and simulated v_{ao} waveforms upto 15^{th} order. The peaks of the fundamental voltage are 101.58 V in experiment, 105 V in simulation which are close to theoretical value, i.e., $150\sqrt{2}\times0.5=106.1$ V. The harmonic spectra of experimental and simulated line currents of ASIM are shown in Fig. 3h and 3k, respectively. The peaks of the fundamental current are 11.73 A in experiment and 10.25 A in simulation. One of the major sources of the non-ideal operation of MC arises during commutation of the four-quadrant switch at low phase current. In that condition, the diode-clamp circuit, as shown in Fig. 13 of [12], comes into play and line-neutral voltage sees a voltage spike. Although the voltage harmonics caused by this non-ideal operation can be low (shown in Fig. 3g, 3j), current harmonics can be significant as the voltage appear in z_1-z_2 plane see very small impedance. Therefore, non-zero current harmonics (shown in Fig. 3h, 3k) and non-zero i_{z_1}, i_{z_2} are resulted due to this non-ideal operation.

The unity power-factor operation in the input is verified from the in-phase v_{Rn} and i_R waveforms which are given in Fig. 3c (experimental) and 3f (simulated). The balanced simulated 3ϕ input currents at input frequency are shown in Fig. 3l. Fig. 3m shows the harmonic spectrum of this input current and it predominantly contains fundamental component with amplitude of 9.4 A. The small deviation of input power-factor angle from zero in Fig. 3c happens due to the input filter used for suppressing switching current ripple at the input port of MC. The input filter configuration is similar to that of Fig. 13 of [12]. The filter inductance, capacitance and resistance values are 6 mH, 90 μF, and 100 Ω, respectively.

Close agreement between simulated and experimental waveforms verifies the proposed modulation strategy.

V. Conclusion

This paper models eighteen switching states of $3\phi-6\phi$ MC, which have zero common-mode voltage, with respect to the standard transformation matrix used for modeling of ASIM. This results into two groups of synchronously rotating space-vectors, each containing 9 states, in both $\alpha-\beta$ and z_1-z_2 planes. The space-vectors generated by states of first group rotate anti-clockwise in $\alpha-\beta$ and clockwise in z_1-z_2. The directions of rotation of the space-vectors of other group are clockwise in $\alpha-\beta$ and anti-clockwise in z_1-z_2. SVPWM techniques for both of these groups are proposed where voltage injection in z_1-z_2 plane is zero and instantaneous common-mode voltage is also zero. If the modulation index is defined as the ratio of peak line-neutral output voltage and peak line-neutral input voltage, maximum modulation index attainable by these techniques is 0.5. Input current analysis of both of these techniques show that the input power-factors are same as load power-factor. In one case, it is leading and in another case, it is lagging. It is shown in the paper that by using both of the groups for half of the sampling period; input power-factor can be maintained at unity.

References

[1] F. Barrero and M. J. Duran, "Recent advances in the design, modeling, and control of multiphase machines—part i," *IEEE Transactions on Industrial Electronics*, vol. 63, no. 1, pp. 449–458, 2015.

[2] P. W. Wheeler, J. Rodriguez, J. C. Clare, L. Empringham, and A. Weinstein, "Matrix converters: A technology review," *IEEE Transactions on industrial electronics*, vol. 49, no. 2, pp. 276–288, 2002.

[3] S. Chen, T. A. Lipo, and D. Fitzgerald, "Source of induction motor bearing currents caused by pwm inverters," *IEEE Transactions on Energy Conversion*, vol. 11, no. 1, pp. 25–32, 1996.

[4] V. Padhee, A. K. Sahoo, and N. Mohan, "Modulation technique for common mode voltage reduction in a matrix converter drive operating with high voltage transfer ratio," in *2016 IEEE Applied Power Electronics Conference and Exposition (APEC)*, pp. 1982–1988. IEEE, 2016.

[5] Y. Zhao and T. A. Lipo, "Space vector pwm control of dual three-phase induction machine using vector space decomposition," *IEEE Transactions on industry applications*, vol. 31, no. 5, pp. 1100–1109, 1995.

[6] K. Marouani, L. Baghli, D. Hadiouche, A. Kheloui, and A. Rezzoug, "A new pwm strategy based on a 24-sector vector space decomposition for a six-phase vsi-fed dual stator induction motor," *IEEE Transactions on Industrial Electronics*, vol. 55, no. 5, pp. 1910–1920, 2008.

[7] A. Bakhshai, G. Joos, and H. Jin, "Space vector pwm control of a split-phase induction machine using the vector classification technique," in *Applied Power Electronics Conference and Exposition, 1998. APEC'98. Conference Proceedings 1998., Thirteenth Annual*, vol. 2, pp. 802–808. IEEE, 1998.

[8] R. Bojoi, A. Tenconi, F. Profumo, G. Griva, and D. Martinello, "Complete analysis and comparative study of digital modulation techniques for dual three-phase ac motor drives," in *Power Electronics Specialists Conference, 2002. pesc 02. 2002 IEEE 33rd Annual*, vol. 2, pp. 851–857. IEEE, 2002.

[9] K. Gopakumar, V. Ranganthan, and S. Bhat, "Split-phase induction motor operation from pwm voltage source inverter," *IEEE Transactions on Industry Applications*, vol. 29, no. 5, pp. 927–932, 1993.

[10] C. Zhou, G. Yang, and J. Su, "Pwm strategy with minimum harmonic distortion for dual three-phase permanent-magnet synchronous motor drives operating in the overmodulation region," *IEEE Transactions on Power Electronics*, vol. 31, no. 2, pp. 1367–1380, 2016.

[11] S. Paul and K. Basu, "Overmodulation techniques of asymmetrical six-phase machine with optimum harmonic voltage injection," *IEEE Transactions on Industrial Electronics*, 2020.

[12] R. K. Gupta, K. K. Mohapatra, A. Somani, and N. Mohan, "Direct-matrix-converter-based drive for a three-phase open-end-winding ac machine with advanced features," *IEEE Transactions on Industrial Electronics*, vol. 57, no. 12, pp. 4032–4042, 2010.

[13] M. A. Sayed and A. Iqbal, "Pulse width modulation technique for a three-to-five phase matrix converter with reduced commutations," *IET Power electronics*, vol. 9, no. 3, pp. 466–475, 2016.